Thin Solid Films 669 (2019) 588–594

Contents lists available at ScienceDirect

Thin Solid Films

journal homepage: www.elsevier.com/locate/tsf

# Water based spray pyrolysis of metal-oxide solutions for $Cu_2ZnSn(S,Se)_4$ solar cells using low toxicity amine/thiol complexants

L.D. Wright[a,*], J.C. Lowe[a,b], M. Bliss[a], V. Tsai[a], M. Togay[a], T.R. Betts[a], J.M. Walls[a], A.V. Malkov[b], J.W. Bowers[a]

[a] Centre for Renewable Energy Systems Technology, Wolfson School of Mechanical, Electrical, and Manufacturing Engineering, Loughborough University, Loughborough, Leicestershire LE113TU, United Kingdom
[b] Department of Chemistry, School of Science, Loughborough University, Loughborough, Leicestershire LE113TU, United Kingdom

ARTICLE INFO

*Keywords:*
Kesterite
Ultrasonic
Spray
Water based
Metal-oxide
Low toxicity
Amine
Thiol

ABSTRACT

$Cu_2ZnSnS(e)_4$ deposited using solution processes has potential for terrawatt-scale deployment. The champion highest efficiency $Cu_2ZnSn(S,Se)_4$ cell published in literature is spin-coated using the highly dangerous hydrazine which is an impractically scalable solvent and deposition combination. As an alternative solvent amine-thiol mixtures have shown to complex with a wide range of binary chalcogenides with much lower health risks than hydrazine. Herein we present two further toxicity reductions, first by employing a less harmful amine-thiol pairing and second by using water as a diluting solvent. We exclude extraneous elements from the precursor solution such as halogens and with a sub-micron thickness crystalline absorber achieve an efficiency of 6.8%. With the modified solution deposited by ultrasonic spray pyrolysis, this solution process is scalable, abundant, and relatively non-toxic.

## 1. Introduction

The sulfide $Cu_2ZnSnS_4$ (CZTS) and selenide $Cu_2ZnSnSe_4$ (CZTSe) combined as the sulfo-selenide $Cu_2ZnSn(S,Se)_4$ (CZTSSe) is a strong contender for terrawatt-scale photovoltaic deployment, with its tunable direct band gap [1,2,3], high absorption coefficient ($> e4\,cm^{-1}$) [4], Earth-abundant material components (unlike the scarce indium in Cu(In,Ga)$Se_2$ (CIGSe) and tellurium in CdTe), and apparent preference for non-vacuum solution processing as shown by its spin-coated 12.6% champion device [5]. The device in question, produced by IBM, uses the solvent hydrazine. Hydrazine has excellent solvent properties as its small molecular weight and volatility means it decomposes cleanly, resulting in contaminant free films. However hydrazineâ€™s toxicity and volatility make it dangerous to work with, as a research tool or for industrial upscale.

The Brutchey group have widely studied the use of amine/thiol mixtures (molecules with functional groups -$NH_2$/-SH, ATMs) for processing semiconductor thin films [6]. Once combined ATMs can complex with a range of elements [7], oxides [8] and dichalcogenides (sulfides, selenides, and tellurides) [9,10,11], and the solutes recoverable upon heating.

ATMs have been used to solution process CZTS(e) solar cells producing efficiencies of 5.1% [12], 6.69% [13], 6.83% [14], 7.66% [15], 7.86% [16,17], and 9.7% [18]. Whilst comparatively less dangerous than hydrazine the choice of ATM (such as ethanolamine/thioglycolic acid [14], hexylamine/propanethiol [16] and ethylenediamine/ethanedithiol [19] have their own associated health risks; the lethal dosages of hydrazine and these ATMs can be seen in Table A1. For terrawatt-scale production a solvent with toxicity as low as possible is ideal, as it reduces the risk to those working with it and the wider environment. Abundance of materials is also key, meaning a water-based solution is preferable.

Thiourea is an amide containing two amine groups which is used widely in the chemical bath deposition of CdS buffer layers [20,21,22,23] and to complex with metal-salts. Salt-solutions are attractive because of their compatibility with a water base and as the precursors are cheap and readily soluble. However, chlorines oxidation state (−1) compared with that of sulfur or selenium (−2) does not fit into the kesterite stoichiometry and so potentially dopes the absorber. Despite this salt solutions have produced device efficiencies such as 3.87% [24], 4.28% [25], 5.1% [26], 6.2% [27], 7.5% [28], 8.6% [29] and 10.8% [30]. A solution route avoiding extraneous elements is desirable.

Previously we have showed the utility of ATMs for processing of

* Corresponding author.
*E-mail address:* l.wright2@lboro.ac.uk (L.D. Wright).

https://doi.org/10.1016/j.tsf.2018.11.040
Received 2 July 2018; Received in revised form 21 November 2018; Accepted 21 November 2018
Available online 26 November 2018

CZTSe [7] and CIGSe [31,32] solar cells using ethanolamine/cysteamine and ethylenediamine/ethanedithiol. For CZTSe cysteamine was chosen due to having a less pungent odour than is expected of thiols, a factor to consider for industry scaling. Ethanolamine however was considered somewhat impractical due to its high viscosity.

Here we present work that combines the amine/thiol and metal-salt routes. We propose for the first time the use of thiourea (TU, amine source) with cysteamine (CA, thiol source) dissolved in water to complex with metal oxides for deposition via ultrasonic spray pyrolysis. The precursors do not contain halogens and dissolve within minutes, while the solution uses water as a base solvent and is deposited by a linearly scalable spraying method.

We demonstrate that 6.8% efficient solar cells are possible using a contaminant free, benign, and environmentally friendly molecular solution route. By staying within the ATM conceptual framework, and probing its lower limits by specifically selecting molecules with low toxicity, we have produced the least toxic ATM reported for thin film semiconductor processing.

## 2. Experimental section

### 2.1. Materials

We purchased the following chemicals from; Sigma Aldrich: cysteamine (CA, 99.2%), thiourea (TU, 99%), zinc oxide (ZnO, 99.99%), tin sulphate ($SnSO_4$, 95%), cadmium sulphate ($CdSO_4$, 99%); Alfa Aesar: copper (II) oxide (CuO, 99.98%), selenium shot (Se shot, 99.999%); Acros Organics: ammonium hydroxide solution ($NH_4OH$, 28–30 wt%). All precursors are used without modification.

### 2.2. Back contact deposition

We DC sputtered the molybdenum (Mo) back contact and molybdenum nitride ($MoN_x$) diffusion barrier onto soda lime glass (SLG). It was deposited with architecture SLG/Mo/$MoN_x$/Mo with respective thicknesses of 1 mm/600 nm/ ~ 30nm/ ~ 50nm [33]. The $MoN_x$ barrier layer is included to prevent excessive $MoSe_2$ formation, which is common during selenisation of solution processed CZTSe and CIGSe solar cells. Controlled formation is necessary as excessive $MoSe_2$ causes device-limiting series resistance [34], while a small amount helps an ohmic contact to form at the semiconductor/metal interface [35].

### 2.3. Solution preparation

We weighed out TU (1.0 g, 13.1 mmol mmol) and CA (1.0 g, 13.0 mmol) in air before adding to DI water (10 ml, 550 mmol) and magnetically stirring to fully dissolve until free of particulates. To this solution we added CuO (0.143 g, 1.8 mmol), ZnO (0.098 g, 1.2 mmol) and $SnSO_4$ (0.215 g, 1.0 mmol). We stirred again until fully dissolved, taking around 5 min, producing to a light yellow solution. Before deposition we diluted with 30 ml DI water and 4.0 g TU. With these precursor masses we targeted metal ratios of $[Zn]/[Sn] = 1.2$ and $[Cu]/[Zn + Sn] = 0.8$.

### 2.4. Deposition and selenisation

We deposited the absorber layer by ultrasonic spray pyrolysis. A hotplate moved underneath the spray nozzle, while the nozzle produced an atomised spray perpendicular to the hotplate. We used $N_2$ gas with a shaping cone attached to the nozzle to direct the spray onto the heated substrate below. The deposition consisted of 12 layers at 1.5 ml $min^{-1}$ onto a hotplate set at 350 °C. The deposition is illustrated in Fig. 1 and full deposition parameters listed in Table 1.

To crystallise the deposition we selenised for 35 min in total at a 575 °C set point. We placed the samples in a a semi-closed graphite box with 12 Se pellets ( ~ 540 mg) and then purged the tube with $N_2$ to set a starting pressure of 10,666 Pa (80 Torr). After the process we cooled the samples naturally. A temperature/pressure profile is shown in Fig. 2.

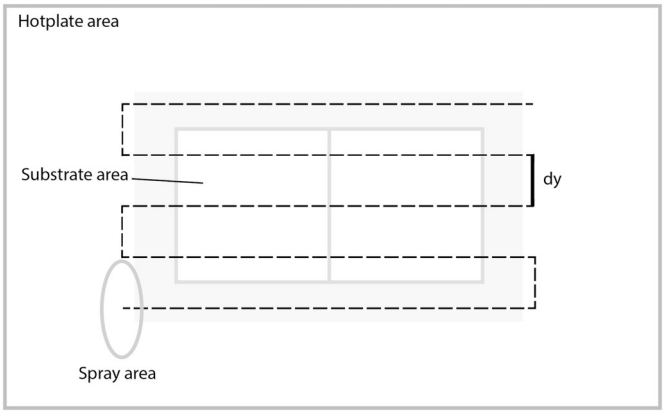


**Fig. 1.** Image showing the motion of the deposition spot over the surface of the hotplate whilst spraying.

**Table 1**
Table of spray deposition parameters.

| Code | Parameter | Units | Value |
|---|---|---|---|
| T | Hotplate | °C | 350 |
| $t_1$ | PreDwell | s | 45 |
| $t_2$ | MidDwell | s | 30 |
| $t_3$ | PostDwell | s | 180 |
| v | Stage speed | mm/s | 40 |
| dy | Sidestep | mm | 10 |
| $r_1$ | Flow rate | ml/min | 1.5 |
| $r_2$ | Gas flow | L/min | 6 |
| p | Power | W | 4.5 |
| n | Layers | – | 12 |
| h | Nozzle height | cm | 5.5 |

We completed devices with a CdS buffer ( ~ 60 nm) by chemical bath deposition (183 ml DI water, 0.015 M $CdSO_4$, 32.6 ml $NH_4OH$, 1.5 M TU, submerged for 10 min at 70 °C), i-ZnO ( ~ 80 nm) and Al:ZnO (500 nm) transparent contacts by RF sputtering and Ag grids (500 nm) by thermal evaporation. After evaporation we scribe the device to produce 16 individual 0.25 $cm^2$ cells.

### 2.5. Characterisation

We took scanning electron microscope (SEM) images and elemental dispersive x-ray spectroscopy (EDS) spectra on a FEGSEM Jeol 7100 at 20 kV acceleration voltage; we measured current density-voltage (JV) curves with a Keithley 2440 5 A sourcemeter, illuminated with an Abet SunLite Solar Simulator and calibrated to 1000 $W/m^2$ with a Si photodiode; we collected external quantum efficiency (EQE) spectra at 0 V bias using a Bentham PVE300 Photovoltaic EQE system with TMc300 monochromator (light source: 75 W Xenon and 100 W Quartz halogen bulb; slit width: 5 mm; spectral resolution: 5 nm, calibrated using a Si and Ge reference diode; we took multiwavelength laser beam induced current (multi-LBIC) measurements with a custom setup consisting of 11 separate laser diodes [36]; we measured spectrally resolved photoluminescence (PL) with a custom built setup [37] using a 640 nm excitation source with laser frequency of 40 MHz.

## 3. Results and discussion

Fig. 3(a) shows an SEM cross-section of the as-deposited sample. The deposition conditions produce an excessively thick 5.8 µm absorber, where individual layers can be seen along with some voids.

The layer effect may be a result of the surface cooling slightly during

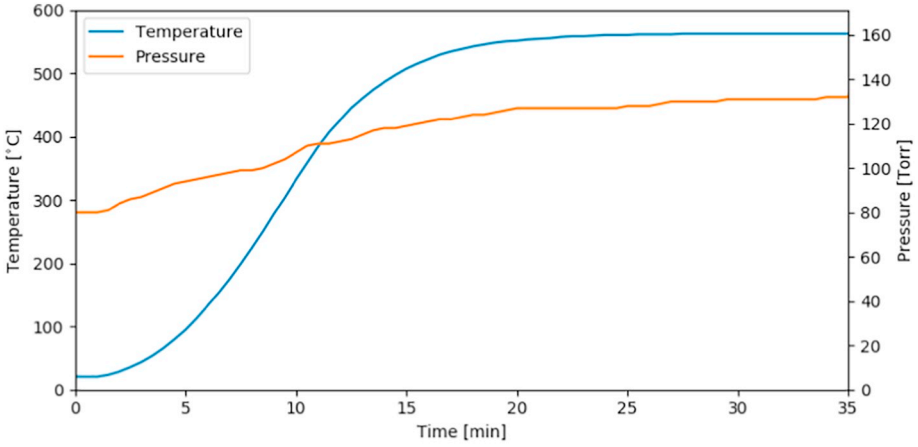


**Fig. 2.** Temperature and pressure profile of selenisation.

deposition due to the shaping gas as the sample moves under the nozzle, resulting in incomplete pyrolysis. The voids may be an extension of this, as poor adhesion from a cooled surface or from carbon attempting to exit the film as a gas during the annealing step between layers. The layers themselves are highly homogeneous which is important for industry scaling. Spray deposition methods such as this are useful for industrial applications as a larger deposition area can be coated by simply adding more spray nozzles.

Fig. 3(b) shows a cross-section of the selenised sample. Here the total thickness has reduced to ~5.6 μm from the as-deposited 5.8 μm. Whilst still highly granular, the bulk appears to have fewer voids and shows a general smoothing between the layers implying a partial crystallisation, both of which could be the source of the thickness reduction.

Crystal formation at the front (400 nm) and back (600 nm) produce the trilayer effect reported previously [28,38,1], notable for solution processed devices. Where reported the layers have a thickness ratio of around 2:1 from top to bottom whereas ours differed slightly at 3:2 ratio. Our films are not intentionally doped, however alkali addition is widely acknowledged as a mechanism for increasing crystallinity [38,39,40] and can be easily implemented in this method.

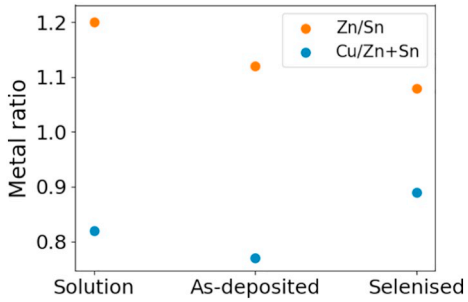


**Fig. 4.** Metal ratios, as calculated from precursor moles for solution and by EDS for the two processing steps.

Fig. 3(c) and (d) show surface images of as-deposited and selenised samples respectively. The as-deposited sample appears grainy and porous, while the selenised sample shows compact crystals with a number of small voids. We suspect these may be 'exhaust' holes, letting out gaseous phases drawn out by the low (partial) pressure in the tube.

EDS shows $[Zn]/[Sn]$ values of 1.12 and 1.08 for the as-deposited

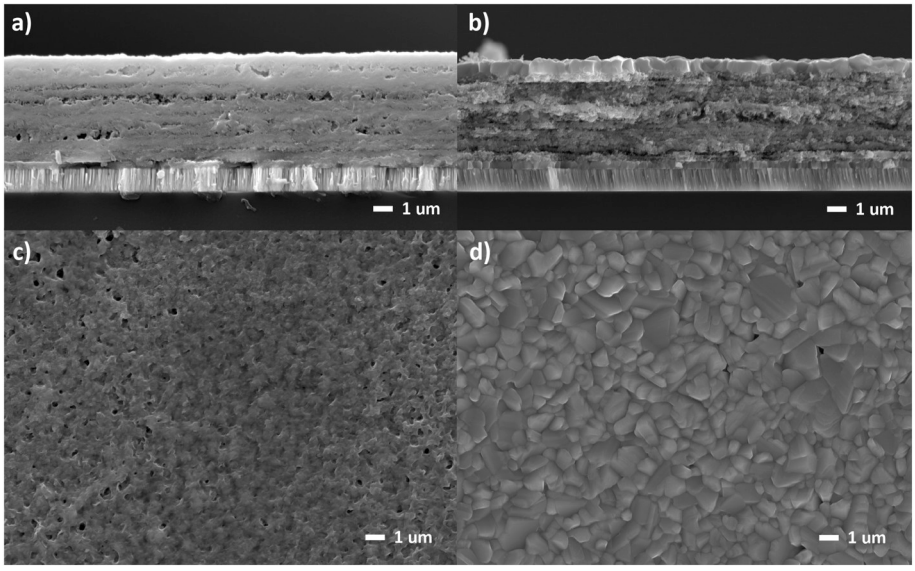


**Fig. 3.** Cross section (a,b) and surface (c,d) SEM images of as-deposited (a,c) and selenised (b,d) CZTS films.

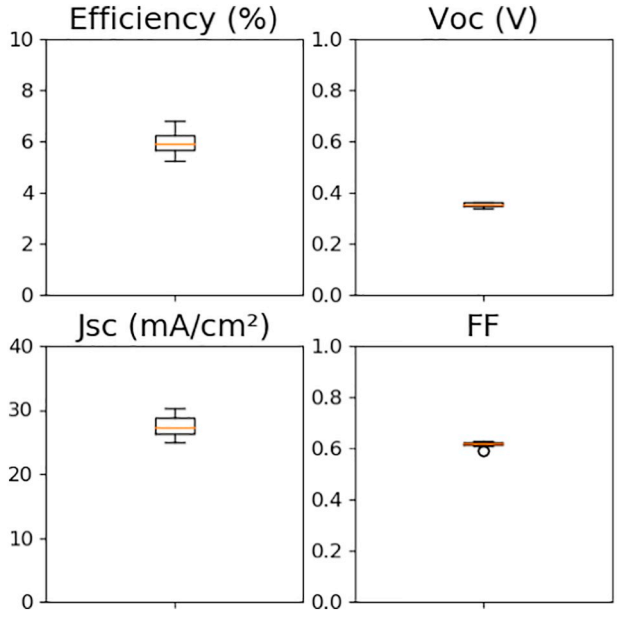


**Fig. 5.** Box plot of all 16 cells for the four main cell parameters.

and selenised films respectively, seen in Fig. 4. Volatile Sn is a major stoichiometric loss mechanism and is to be expected when selenising without an excess Sn atmosphere [41]. Here however more Zn is lost than Sn. The exact nature of the metal complexes in solution is largely unknown, so it is possible some highly volatile Zn phase is formed and lost, partly during deposition and partly during selenisation.

$[Cu]/[Zn + Sn]$ EDS ratios of 0.77 and 0.89 suggest a reduction in Cu after depositing the solution but a loss of Zn and/or Sn after selenising. Despite their changing value, both ratios are within expectation for high performance kesterite solar cells, namely a Cu-poor/Zn-rich stoichiometry [42,43].

EDS also shows a consistently high (~40 at.%) carbon content. This is from the thick uncrystallised layer and can be effectively reduced by lowering the number of deposition layers.

Fig. 5 shows a box plot of the main parameters (efficiency ($\eta$), open-circuit voltage ($V_{oc}$), short-circuit current ($J_{sc}$) and fill factor ($FF$)) for all 16 cells; the average values for each parameter are: $\eta = 6.0\%$, $V_{oc} = 352$ mV, $J_{sc} = 27.4$ mA/cm$^2$, and $FF = 62\%$. From Fig. 5 it can be seen that the variation in efficiency is mainly due to variations in the $J_{sc}$,

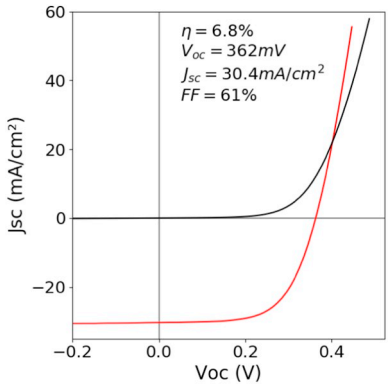


**Fig. 6.** Current density-voltage curve for the champion cell.

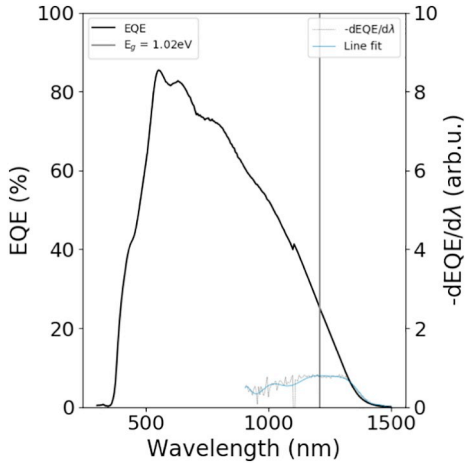


**Fig. 7.** External quantum efficiency curve for the champion cell.

with low variation in the $V_{oc}$ or $FF$. All cells exhibit the typically low $V_{oc}$ characteristic of selenium rich kesterites.

Fig. 6 shows dark and light curves of the champion cell, with key parameters of $\eta = 6.8\,\%$, $V_{oc} = 362$ mV, $J_{sc} = 30.4$ mA/cm$^2$, and $FF = 61\%$.

With the exception of the barrier layer (which appears not to have been needed due to the lack of $MoSe_2$) this method has no additional processing steps such as air- or device stack-annealing, doping, intermediate layers, or changes in initial stoichiometry. Notable as well is that this is from spray deposition, which despite its clear industrial benefits has historically performed poorly [44].

To examine the spectral response the EQE was measured with bias light, shown in Fig. 7. It initially reaches 85% EQE at ~500 nm but then reduces almost linearly to zero. Low crystalinity in the bulk results in poor collection at longer wavelengths, and implies that the performance is due mostly to the top layer of crystals. A dotted line in Fig. 7 shows a plot of $-dEQE/d\lambda$, with the blue line showing an approximate fit, the peak of which gives an approximation of the absorber band gap.

Spatially resolved multi-LBIC in Fig. 8 over a range of wavelengths agrees with what is seen in Fig. 7; an initially low conversion efficiency then peaks at above 80% with a gradual decline towards longer wavelengths. Apart from a number of bright patches at 405 nm the cell shows a homogeneous response across the whole area for all wavelengths. A number of dark spots can also be seen across all wavelengths suggesting low photoactivity which could be related to secondary phases and/or pinholes.

Room temperature PL is taken to estimate the band gap with more confidence, as seen in Fig. 9. The data is normalised and then smoothed using a Savizky-Golay filter (data points $(p) = 851$, window length $= \sqrt{p}$, polynomial order = 1). Smoothing highlights the general trajectory of the data while highlighting a large peak at 0.95 eV and some shallower responses between 1.25 eV and 1.70 eV. The main peak is attributed to the top crystal layer in Fig. 3(b) and from the band gap is assumed to be pure CZTSe. The peak indicates a band gap value in reasonable agreement with that of $-dEQE/d\lambda$ interpretation, however here the PL value is considered the most accurate due to the wide peak produced by the gradient of the EQE.

Raw data files can be found in the Loughborough data repository [45].

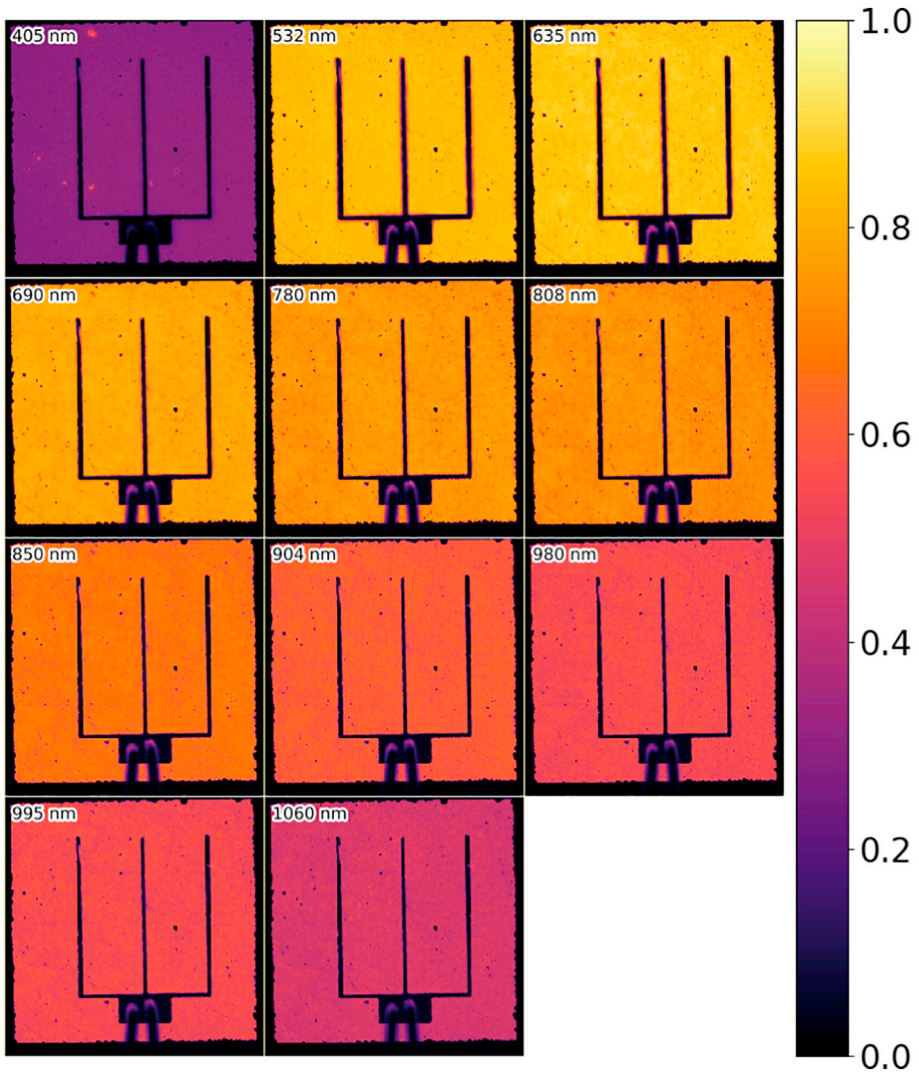


**Fig. 8.** Plots showing spatially resolved LBIC at various laser wavelengths of the champion cell.

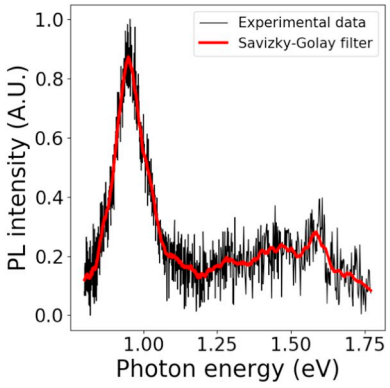


**Fig. 9.** Photoluminescence spectrum for the champion cell.

## 4. Conclusions

In summary, we present a water-based molecular solution for depositing CZTSSe solar cells via ultrasonic spray pyrolysis. After processing, the absorber gives 6.8% conversion efficiency. A large absorber produces a thin (< 1 μm) upper crust of CZTSe, on top of a highly carbon-rich uncrystallised layer. Despite this EQE shows 85% collection at shorter wavelengths. The amine-thiol mixture used to dissolve the metal-oxide precursors is the least toxic combination reported, and is industrially scalable thanks to its water base and spray deposition. This shows the feasibility of safer solution processes. Modifications such as thinner absorber layer and alkali doping to increase crystallinity are expected to further boost device performance, while retaining the benefits of a non-toxic solution route.

## Acknowledgements

The authors would like to acknowledge the EPSRC for funding through the Centre for Doctoral Training in New and Sustainable Photovoltaics [grant number EP/L01551X/1] and The PVTEAM project [grant number EP/L017792/1] to support this work. The authors acknowledge use of facilities within the Loughborough Materials Characterisation Centre.

## Appendix A. Appendix

Table A1
Table of lethal dosages for hydrazine and a number of amine/thiol mixtures.

| | CAS chemical units | 302-01-2 Hydrazine | 107-15-3 Ethylenediamine | 540-63-6 Ethanedithiol | 141-43-5 Ethanolamine | 68-11-1 Thioglycolic// acid | 111-26-2 Hexylamine | 107-03-9 Propanethiol | 62-56-6 Thiourea | 60-23-1 Cysteamine |
|---|---|---|---|---|---|---|---|---|---|---|
| LD50 RAT-ORL | mg/kg | 60 | 500 | 144[1], 120[2] | 1089[1] | 114[1, 2] | 670[2] | 1730 | 1750[1], 20[2], 125–1930[3] | – |
| LC50 RAT-INH | ppm/4 h | 570 | – | 2[1] | – | 290[1] | – | 7300 | 55[1] | – |
| LD50 RAT-IPR | mg/kg | 59 | 76 | – | 67[2] | 70[2] | – | 515 | 436[2] | 232[2] |
| LD50 RAT-IVN | mg/kg | 55 | – | – | 225[2] | – | – | – | – | – |
| LD50 RAT-SCU | mg/kg | – | 300 | – | – | – | – | – | – | 84[2] |
| LD50 MUS-ORL | mg/kg | 59 | – | – | 700[2] | 242[2] | – | – | ~1000[3], ~8500[4] | 625[1, 2] |
| LC50 MUS-INH | ppm/4 h | 252 | – | – | – | – | – | 4010 | – | – |
| LD50 MUS-IPR | mg/kg | 62 | 200 | 50[3] | 50[2] | 138[2] | – | – | – | 250[2] |
| LD50 MUS-IVN | mg/kg | 57 | – | 56[3] | – | 145[2] | – | – | – | 190[2] |
| LD50 MUS-SCU | mg/kg | – | 424 | – | – | – | – | – | – | 84[2] |
| LD50 RAB-DER | mg/kg | 91 | 730 | 197[1, 2] | 1015[1] | 848[1] | 420[1] | – | > 2800 | – |
| | Ref | [46] | [46] | 1[47]; 2[48]; 3[49] | 1[47], 2[49] | 1[47], 2[49] | 1[47]; 2[50] | [46] | 1[47]; 2[51]; 3[52], 4[53] | 1[47]; 2[54] |

LD - Lethal dose kills 50%; LC - Lethal concentration kills 50%; MUS - Mouse; RAT - Rat; RAB - Rabbit; ORL - Oral; INH - Inhalation; IPR - Intraperitoneal; IVN - Intravenous; DER - Dermal; SCU - Subcutaneous.

## References


[1] M. Neuwirth, E. Seydel, J. Seeger, A. Welle, H. Kalt, M. Hetterich, Band-gap tuning of $Cu_2ZnSn(S,Se)_4$ solar cell absorbers via defined incorporation of sulfur based on a post-sulphurization process, Sol. Energy Mater. Sol. Cells 182 (2018) 158–165, https://doi.org/10.1016/j.solmat.2018.03.033 http://linkinghub.elsevier.com/retrieve/pii/S0927024818301429.

[2] S. Ahn, S. Jung, J. Gwak, A. Cho, K. Shin, K. Yoon, D. Park, H. Cheong, J.H. Yun, Determination of band gap energy (Eg) of $Cu_2ZnSnSe_4$ thin films: On the discrepancies of reported band gap values, Appl. Phys. Lett. 97 (2) (2010) 021905, https://doi.org/10.1063/1.3457172 http://aip.scitation.org/doi/10.1063/1.3457172.

[3] C. Malerba, F. Biccari, C.L. Azanza Ricardo, M. Valentini, R. Chierchia, M. Müller, A. Santoni, E. Esposito, P. Mangiapane, P. Scardi, A. Mittiga, CZTS stoichiometry effects on the band gap energy, J. Alloys Compd. 582 (2014) 528–534, https://doi.org/10.1016/j.jallcom.2013.07.199 http://ieeexplore.ieee.org/document/6318212/http://linkinghub.elsevier.com/retrieve/pii/S0925838813018343.

[4] H. Katagiri, K. Jimbo, Fabrication of earth-abundant CZTS thin film solar cells, 2016 23rd International Workshop on Active-Matrix Flatpanel Displays and Devices (AM-FPD), IEEE, 2016, pp. 54–55, https://doi.org/10.1109/AM-FPD.2016.7543617 http://ieeexplore.ieee.org/document/7543617/.

[5] W. Wang, M.T. Winkler, O. Gunawan, T. Gokmen, T.K. Todorov, Y. Zhu, D.B. Mitzi, Device characteristics of CZTSSe thin-film solar cells with 12.6% efficiency, Adv. Energy Mater. 4 (7) (2014) 1301465, https://doi.org/10.1002/aenm.201301465 http://doi.wiley.com/10.1002/aenm.201301465.

[6] D.H. Webber, R.L. Brutchey, Alkahest for $V_2VI_3$ chalcogenides: dissolution of nine bulk semiconductors in a diamine-dithiol solvent mixture, J. Am. Chem. Soc. 135 (42) (2013) 15722–15725, https://doi.org/10.1021/ja4084336 http://pubs.acs.org/doi/10.1021/ja4084336.

[7] C.S. Cooper, P. Arnou, L.D. Wright, S. Uličná, J.M. Walls, A.V. Malkov, J.W. Bowers, An innovative approach for fabrication of $Cu_2ZnSnSe_4$ absorber layers using solutions of elemental metal powders, Thin Solid Films 633 (2017) 151–155, https://doi.org/10.1016/j.tsf.2016.12.026 http://linkinghub.elsevier.com/retrieve/pii/S0040609016308392.

[8] C.L. McCarthy, D.H. Webber, E.C. Schueller, R.L. Brutchey, Solution-phase conversion of bulk metal oxides to metal chalcogenides using a simple thiol-amine solvent mixture, Angew. Chem. Int. Ed. 54 (29) (2015) 8378–8381, https://doi.org/10.1002/anie.201503353 http://doi.wiley.com/10.1002/anie.201503353.

[9] D.H. Webber, J.J. Buckley, P.D. Antunez, R.L. Brutchey, Facile dissolution of selenium and tellurium in a thiolamine solvent mixture under ambient conditions, Chem. Sci. 5 (6) (2014) 2498, https://doi.org/10.1039/c4sc00749b http://xlink.rsc.org/?DOI=c4sc00749b.

[10] C.L. McCarthy, P. Cottingham, K. Abuyen, E.C. Schueller, S.P. Culver, R.L. Brutchey, Earth abundant $CuSbS_2$ thin films solution processed from thiolamine mixtures, J. Mater. Chem. C 4 (26) (2016) 6230–6233, https://doi.org/10.1039/C6TC02117D http://xlink.rsc.org/?DOI=C6TC02117D.

[11] C.L. McCarthy, R.L. Brutchey, Solution processing of chalcogenide materials using thiolamine alkahest solvent systems, Chem. Commun. 53 (36) (2017) 4888–4902, https://doi.org/10.1039/C7CC02226C http://xlink.rsc.org/?DOI=C7CC02226C.

[12] X. Zeng, K.F. Tai, T. Zhang, C.W.J. Ho, X. Chen, A. Huan, T.C. Sum, L.H. Wong, $Cu_2ZnSn(S,Se)_4$ kesterite solar cell with 5.1% efficiency using spray pyrolysis of aqueous precursor solution followed by selenization, Sol. Energy Mater. Sol. Cells 124 (2014) 55–60, https://doi.org/10.1016/j.solmat.2014.01.029 http://linkinghub.elsevier.com/retrieve/pii/S0927024814000464.

[13] Y. Yang, X. Kang, L. Huang, S. Wei, D. Pan, A general water-based precursor solution approach to deposit earth abundant $Cu_2ZnSn(S,Se)_4$ thin film solar cells, J. Power Sources 313 (2016) 15–20, https://doi.org/10.1016/j.jpowsour.2016.01.085 http://linkinghub.elsevier.com/retrieve/pii/S0378775316300854.

[14] Q. Tian, G. Wang, W. Zhao, Y. Chen, Y. Yang, L. Huang, D. Pan, Versatile and low-toxic solution approach to binary, ternary, and quaternary metal sulfide thin films and its application in $Cu_2ZnSn(S,Se)_4$ solar cells, Chem. Mater. 26 (10) (2014) 3098–3103, https://doi.org/10.1021/cm5002412 http://pubs.acs.org/doi/10.1021/cm5002412.

[15] K. Liu, B. Yao, Y. Li, Z. Ding, H. Sun, Y. Jiang, G. Wang, D. Pan, A versatile strategy for fabricating various $Cu_2ZnSnS_4$ precursor solutions, J. Mater. Chem. C 5 (12) (2017) 3035–3041, https://doi.org/10.1039/C6TC04992C http://xlink.rsc.org/?DOI=C6TC04992C.

[16] R. Zhang, S.M. Szczepaniak, N.J. Carter, C.A. Handwerker, R. Agrawal, A versatile solution route to efficient $Cu_2ZnSn(S,Se)_4$ thin-film solar cells, Chem. Mater. 27 (6) (2015) 2114–2120, https://doi.org/10.1021/cm504654t http://pubs.acs.org/doi/10.1021/cm504654t.

[17] X. Zhao, R. Zhang, C. Handwerker, R. Agrawal, The potential of aminethiol based solution processing for chalcogenide photovoltaics, 2016 IEEE 43rd Photovoltaic Specialists Conference (PVSC), IEEE, 2016, pp. 0542–0544, https://doi.org/10.1109/PVSC.2016.7749653 http://ieeexplore.ieee.org/document/7749653/.

[18] J. Fu, J. Fu, Q. Tian, H. Wang, F. Zhao, J. Kong, X. Zhao, S. Wu, Tuning the Se Content in Cu2ZnSn(S, Se)4 Absorber to Achieve 9.7% Solar Cell Efficiency from a Thiol/Amine-Based Solution Process, ACS Appl. Energy Mater. (2018), https://doi.org/10.1021/acsaem.7b00146.

[19] Z. Lin, Q. He, A. Yin, Y. Xu, C. Wang, M. Ding, H.-C. Cheng, B. Papandrea, Y. Huang, X. Duan, Cosolvent approach for solution-processable electronic thin films, ACS Nano 9 (4) (2015) 4398–4405, https://doi.org/10.1021/acsnano.5b00886 http://pubs.acs.org/doi/10.1021/acsnano.5b00886.

[20] F. Lisco, P. Kaminski, A. Abbas, K. Bass, J. Bowers, G. Claudio, M. Losurdo, J. Walls, The structural properties of CdS deposited by chemical bath deposition and pulsed direct current magnetron sputtering, Thin Solid Films 582 (2015) 323–327, https://doi.org/10.1016/j.tsf.2014.11.062 http://linkinghub.elsevier.com/retrieve/pii/S0040609014012176.

[21] Y. Sánchez, M. Espíndola-Rodríguez, H. Xie, S. López-Marino, M. Neuschitzer, S. Giraldo, M. Dimitrievska, M. Placidi, V. Izquierdo-Roca, F. Pulgarín-Agudelo, O. Vigil-Galán, E. Saucedo, Ultra-thin CdS for highly performing chalcogenides thin film based solar cells, Sol. Energy Mater. Sol. Cells 158 (2016) 138–146, https://doi.org/10.1016/j.solmat.2015.12.037 http://linkinghub.elsevier.com/retrieve/pii/S0927024815006856.

[22] K. Ramanathan, M.A. Contreras, C.L. Perkins, S. Asher, F.S. Hasoon, J. Keane, D. Young, M. Romero, W. Metzger, R. Noufi, J. Ward, A. Duda, Properties of 19.2% efficiency ZnO/CdS/$CuInGaSe_2$ thin-film solar cells, Prog. Photovolt. Res. Appl. 11 (4) (2003) 225–230, https://doi.org/10.1002/pip.494 http://doi.wiley.com/10.1002/pip.494.

[23] H.-N. Cui, S.-Q. Xi, The fabrication of dipped CdS and sputtered ITO thin films for

photovoltaic solar cells, Thin Solid Films 288 (1–2) (1996) 325–329, https://doi.org/10.1016/S0040-6090(96)08825-6 http://linkinghub.elsevier.com/retrieve/pii/S0040609096088256.
[24] H. Chen, Q. Ye, X. He, J. Ding, Y. Zhang, J. Han, J. Liu, C. Liao, J. Mei, W. Lau, Electrodeposited CZTS solar cells from Reline electrolyte, Green Chem. 16 (8) (2014) 3841–3845, https://doi.org/10.1039/C4GC00142G http://xlink.rsc.org/?DOI=C4GC00142G.
[25] C.M. Fella, A.R. Uhl, Y.E. Romanyuk, A.N. Tiwari, $Cu_2ZnSnSe_4$ absorbers processed from solution deposited metal salt precursors under different selenization conditions, Phys. Status Solidi A 209 (6) (2012) 1043–1048, https://doi.org/10.1002/pssa.201228003 http://doi.wiley.com/10.1002/pssa.201228003.
[26] Z. Su, K. Sun, Z. Han, H. Cui, F. Liu, Y. Lai, J. Li, X. Hao, Y. Liu, M.A. Green, Fabrication of $Cu_2ZnSnS_4$ solar cells with 5.1% efficiency via thermal decomposition and reaction using a non-toxic solgel route, J. Mater. Chem. A 2 (2) (2014) 500–509, https://doi.org/10.1039/C3TA13533K http://xlink.rsc.org/?DOI=C3TA13533K.
[27] M. Jiang, F. Lan, X. Yan, G. Li, $Cu_2ZnSn(S_{1-x}Se_x)_4$ thin film solar cells prepared by water-based solution process, Phys. Status Solidi (RRL) 8 (3) (2014) 223–227, https://doi.org/10.1002/pssr.201308215 http://doi.wiley.com/10.1002/pssr.201308215.
[28] T. Schnabel, M. Löw, E. Ahlswede, Vacuum-free preparation of 7.5% efficient $Cu_2ZnSn(S,Se)_4$ solar cells based on metal salt precursors, Sol. Energy Mater. Sol. Cells 117 (2013) 324–328, https://doi.org/10.1016/j.solmat.2013.06.021 http://linkinghub.elsevier.com/retrieve/pii/S0927024813003061.
[29] G. Larramona, S. Bourdais, A. Jacob, C. Choné, T. Muto, Y. Cuccaro, B. Delatouche, C. Moisan, D. Péré, G. Dennler, 8.6% Efficient CZTSSe solar cells sprayed from water-ethanol CZTS colloidal solutions, J. Phys. Chem. Lett. 5 (21) (2014) 3763–3767, https://doi.org/10.1021/jz501864a http://pubs.acs.org/doi/10.1021/jz501864a.
[30] G. Larramona, S. Levcenko, S. Bourdais, A. Jacob, C. Choné, B. Delatouche, C. Moisan, J. Just, T. Unold, G. Dennler, Fine-tuning the Sn content in CZTSSe thin films to achieve 10.8% solar cell efficiency from spray-deposited water-ethanol-based colloidal inks, Adv. Energy Mater. 5 (24) (2015) 1501404, https://doi.org/10.1002/aenm.201501404 http://doi.wiley.com/10.1002/aenm.201501404.
[31] P. Arnou, C.S. Cooper, S. Uličná, A. Abbas, A. Eeles, L.D. Wright, A.V. Malkov, J.M. Walls, J.W. Bowers, Solution processing of $CuIn(S,Se)_2$ and $Cu(In,Ga)(S,Se)_2$ thin film solar cells using metal chalcogenide precursors, Thin Solid Films 633 (2017) 76–80, https://doi.org/10.1016/j.tsf.2016.10.011 https://linkinghub.elsevier.com/retrieve/pii/S0040609016305995.
[32] S. Uličná, P. Arnou, C.S. Cooper, L.D. Wright, A.V. Malkov, M. Walls, J.W. Bowers, Hydrazine-free metal chalcogenide precursor solutions for sprayed $CuIn(S,Se)_2$ thin film solar cells, 12th Photovoltaic Science, Application and Technology Conference C98, 2016 https://dspace.lboro.ac.uk/2134/24320.
[33] S. Uličná, P. Arnou, A. Eeles, M. Togay, L.D. Wright, A. Abbas, A.V. Malkov, M. Walls, J.W. Bowers, Control of $MoSe_2$ formation in hydrazinefree solution-processed CIS/CIGS thin film solar cells, IEEE Photovoltaic Specialists Conference (PVSC), 2017 https://dspace.lboro.ac.uk/2134/25996.
[34] J. Li, Y. Zhang, W. Zhao, D. Nam, H. Cheong, L. Wu, Z. Zhou, Y. Sun, A temporary barrier effect of the alloy layer during selenization: tailoring the thickness of $MoSe_2$ for efficient $Cu_2ZnSnSe_4$ solar cells, Adv. Energy Mater. 5 (9) (2015) 1402178, https://doi.org/10.1002/aenm.201402178 http://doi.wiley.com/10.1002/aenm.201402178.
[35] B. Shin, N.A. Bojarczuk, S. Guha, On the kinetics of $MoSe_2$ interfacial layer formation in chalcogen-based thin film solar cells with a molybdenum back contact, Appl. Phys. Lett. 102 (9) (2013) 091907, https://doi.org/10.1063/1.4794422 http://aip.scitation.org/doi/10.1063/1.4794422.
[36] M. Bliss, G. Koutsourakis, T.R. Betts, R. Gottschalg, Development of a solar cell spectral response mapping system using multi-LBIC excitation, The 12th Photovoltaic Science, Application and Technology Conference, 2016 https://dspace.lboro.ac.uk/2134/22859.
[37] V. Tsai, F. Bittau, C. Potamialis, M. Bliss, T.R. Betts, R. Gottschalg, Combined electrical and optical characterisation of recombination mechanisms and minority carrier lifetime in solar cells, 14th Photovoltaic Science, Applications and Technology Conference, 2018.
[38] T. Abzieher, T. Schnabel, M. Hetterich, M. Powalla, E. Ahlswede, Source and effects of sodium in solution-processed kesterite solar cells, Phys. Status Solidi A 213 (4) (2016) 1039–1049, https://doi.org/10.1002/pssa.201532619 http://doi.wiley.com/10.1002/pssa.201532619.
[39] G. Altamura, M. Wang, K.-L. Choy, Influence of alkali metals (Na, Li, Rb) on the performance of electrostatic spray-assisted vapor deposited $Cu_2ZnSn(S,Se)_4$ solar cells, Sci. Rep. 6 (1) (2016) 22109, https://doi.org/10.1038/srep22109 http://www.nature.com/articles/srep22109.
[40] C. Andres, T. Schwarz, S. Haass, T. Weiss, R. Carron, R. Caballero, R. Figi, C. Schreiner, M. Bürki, A. Tiwari, Y. Romanyuk, Decoupling of optoelectronic properties from morphological changes in sodium treated kesterite thin film solar cells, Sol. Energy (2018), https://doi.org/10.1016/j.solener.2018.03.067 http://linkinghub.elsevier.com/retrieve/pii/S0038092X18302986.
[41] A. Redinger, D.M. Berg, P.J. Dale, S. Siebentritt, The Consequences of kesterite equilibria for efficient solar cells, J. Am. Chem. Soc. 133 (10) (2011) 3320–3323, https://doi.org/10.1021/ja111713g http://pubs.acs.org/doi/abs/10.1021/ja111713g.
[42] A.D. Collord, H. Xin, H.W. Hillhouse, Combinatorial exploration of the effects of intrinsic and extrinsic defects in $Cu_2ZnSn(S,Se)_4$, IEEE J. Photovolt. 5 (1) (2015) 288–298, https://doi.org/10.1109/JPHOTOV.2014.2361053 http://ieeexplore.ieee.org/lpdocs/epic03/wrapper.htm?arnumber=6945352.
[43] T.K. Todorov, K.B. Reuter, D.B. Mitzi, High-efficiency solar cell with earth-abundant liquid-processed absorber, Adv. Mater. 22 (20) (2010) E156–E159, https://doi.org/10.1002/adma.200904155 http://doi.wiley.com/10.1002/adma.200904155.
[44] M. Courel, E. Valencia-Resendiz, J. Andrade-Arvizu, E. Saucedo, O. Vigil- Galán, Towards understanding poor performances in spray-deposited $Cu_2ZnSnS_4$ thin film solar cells, Sol. Energy Mater. Sol. Cells 159 (2017) 151–158, https://doi.org/10.1016/j.solmat.2016.09.004 http://linkinghub.elsevier.com/retrieve/pii/S0927024816303312.
[45] L.D. Wright, Data and Images, (2018), https://doi.org/10.17028/rd.lboro.c.4299728.v1 https://figshare.com/collections/Data_and_images_for_Water_based_spray_pyrolysis_of_metal-oxide_solutions_for_CZTSSe_solar_cells_using_low_toxicity_amine_thiol_complexants_/4299728/1.
[46] U.S. National Library of Medicine, WebWISER, https://webwiser.nlm.nih.gov.
[47] Sigma Alrdich, Safety Data Sheet, https://www.sigmaaldrich.com/united-kingdom.html.
[48] E. Bingham, B. Cohrssen, C. Powell, Patty's Toxicology Volumes 1–9, 5th edition, vol. 7, John Wiley & Sons, New York, N.Y., 2001.
[49] R.J. Lewis (Ed.), Sax's Dangerous Properties of Industrial Materials, John Wiley & Sons, Inc., Hoboken, NJ, USA, 2004, https://doi.org/10.1002/0471701343 http://doi.wiley.com/10.1002/0471701343.
[50] ScienceLab, Safety Data Sheet, http://www.sciencelab.com.
[51] I. Toxic, Hazardous Industrial Chemicals Safety Manual, The International Technical Information Institute, Tokyo, 1988.
[52] WHO/Internatinal Programme on Chemical Safety, Concise international chemical assessment, Tech. Rep. (2003), www.inchem.org/pages/hsg.html.
[53] European Commission ESIS, IUCLID dataset, CD ROM edition, Tech. Rep. (2009) Available from http://esis.jrc.ec.europa.eu.
[54] Sigma Aldrich, Historical cysteamine SDS, Tech. Rep. (2006). URL http://play.psych.mun.ca/$\sim$smilway/MSDS/mercaptoethylamine.pdf